JACS
JOURNAL OF THE AMERICAN CHEMICAL SOCIETY
Article
pubs.acs.org/JACS

Sunlight-Triggered Nanoparticle Synergy: Teamwork of Reactive Oxygen Species and Nitric Oxide Released from Mesoporous Organosilica with Advanced Antibacterial Activity

Julia Gehring,[†] Bastian Trepka,[†] Nele Klinkenberg,[†] Hannah Bronner,[†] David Schleheck,[‡] and Sebastian Polarz*[,†]

[†]Department of Chemistry and [‡]Department of Biology, University of Konstanz, Konstanz D-78457, Germany

Supporting Information

ABSTRACT: Colonization of surfaces by microorganisms is an urging problem. In combination with the increasing antibiotic resistance of pathogenic bacteria, severe infections are reported more frequently in medical settings. Therefore, there is a large demand to explore innovative surface coatings that provide intrinsic and highly effective antibacterial activity. Materials containing silver nanoparticles have been developed in the past for this purpose, but this solution has come into criticism due to various disadvantages like notable toxicity against higher organisms, the high price, and low abundance of silver. Here, we introduce a new, sunlight-mediated organosilica nanoparticle (NP) system based on silver-free antibacterial activity. The simultaneous release of nitric oxide (NO) in combination with singlet oxygen and superoxide radicals ($O_2^{\bullet -}$) as reactive oxygen species (ROS) leads to the emergence of highly reactive peroxynitrite molecules with significantly enhanced biocidal activity. This special cooperative effect can only be realized, if the ROS-producing moieties and the functional entities releasing NO are spatially separated from each other. In one type of particle, Rose Bengal as an efficient singlet oxygen ($^1O_2$) producer was covalently bound to SH functionalities applying thiol−ene click chemistry. "Charging" the second type of particles with NO was realized by quantitatively transferring the thiol groups into *S*-nitrosothiol functionalities. We probed the oxidation power of ROS-NP alone and in combination with NO-NP using sunlight as a trigger. The high antibacterial efficiency of dual-action nanoparticles was demonstrated using disinfection assays with the pathogenic bacterium *Pseudomonas aeruginosa*.

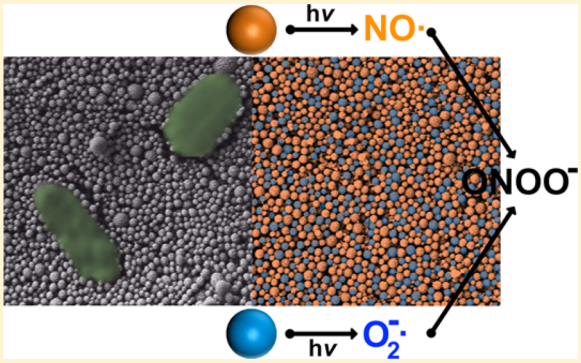

INTRODUCTION

Pathogenic microorganisms are the second largest cause of death worldwide with 17 million annual victims.[1] In particular, colonization of bacteria on surfaces in medical facilities and accidental infections represents a severely increasing problem. To address this issue, two main strategies currently exist. Considerable effort is made to either inactivate the pathogenic microorganisms or kill them, for example, by application of new types of antibiotics.[2,3] A second strategy for controlling pathogenic infections is by means of preventing the settlement, growth, and colonization of microorganism on biorelevant surfaces.[3−5] Systems based on silver nanoparticles still represent the most popular antibacterial agent platform,[6] but there are serious reasons as to why there is a need for alternatives. Besides the antibacterial activity of silver, it shows unacceptable toxic effects on human health (argyria) and environment.[7] With a natural abundance in the earth crust of only 0.075 ppm, it belongs to the rare elements, which aggravates its application in mass technology. A promising alternative for antibacterial surface protection was introduced very recently: antibacterial photodynamic therapy (APDT).[8] This unique approach is based on the use of photoactive substances, respectively, photosensitizers (PS), which by absorbing visible light lead to the generation of reactive oxygen species (ROS) like hydrogen peroxide, hydroxyl radicals, superoxide radicals, or singlet oxygen.[9] These reactive states of oxygen react with a large number of biological substrates like DNA, RNA, and proteins.[10] The consequence is harmful damage to the cell membrane and cellular walls, finally ending in cell death.

The efficiency of APDT strongly depends on the quality of the applied PS. A high absorption coefficient, high photostability, and no toxicity in the dark characterize an efficient APDT-PS.[11] Rose Bengal (RB) is known as an excellent PS as its absorption bands are located in the visible range between 480 and 550 nm and its singlet oxygen production yield is very high ($\Phi(^1O_2) = 0.75$).[11,12] Via incorporation of RB in materials like polymers,[13] metals,[14] or silica,[11,15] its photostability can increase tremendously.[16] Regarding NO storage, the work of Schoenfisch et al. on different NO donors covalently bound to surfaces is worth mentioning.[17−19]

Received: November 18, 2015
Published: February 17, 2016

DOI: 10.1021/jacs.5b12073
J. Am. Chem. Soc. 2016, 138, 3076−3084

Recent reports show that mesoporous silica nanoparticles (MSN) possess a vast potential for applications in biological systems,[20] which is attributed to their very high internal surface area (1500 m^2/g) as well as their potential of being modified with a broad range of organic functionalities.[21] By grafting or co-condensation, a variety of organic entities can be introduced, and the reader is referred to the recent review articles covering this field.[22,23] Materials with a much higher degree of organic functionalization (up to 100%), so-called PMOs (periodically mesoporous organosilica), can be obtained, when special sol−gel precursors with bridging organic groups ($(R'O)_3Si-R-Si(OR')_3$) are used.[24−27] Unfortunately, the number of examples of MSNs of the PMO type is very low and restricted to precursors of very limited chemical functionality.[28,29] Therefore, it is highly desirable to produce PMO-MSNs containing functional groups in the materials.[30] To address this issue, we recently presented organosilica materials with bridging, functionalized phenyl derivatives, the so-called UKON materials.[31−35] The materials were also tested concerning their potential for antibacterial applications.[36,37] In this context, we showed that 100% functionalization is indispensable to prevent fouling.

The limitation of all systems presented in literature until now is the low density of functional groups, which are capable of covalently binding photosensitizers as well as NO. Hence, it can be expected that the application of the PMO technology to this field would be very beneficial, and in particular PMO-MSNs with thiol groups[38] are promising candidates for the incorporation of ROS- and NO- functions.[39−41] Therefore, our research program for this Article is defined as follows: Our first goal was to establish the Stoeber method for the generation of thiol-containing PMO-MSNs. We then wanted to study the modification of these novel PMO particles with ROS-producing and NO-binding functionalities and characterize their photochemical properties. However, an even more challenging goal should be realized. We want to explore potential cooperative effects resulting from the combination of the two mentioned functional entities.

RESULTS AND DISCUSSION

Preparation of Thiol Functionalized PMO Nanoparticles via a Modified Stoeber Method. In our previous study, the synthesis of highly porous thiol PMO nanoparticles in the range from 100 nm to 1 μm was performed by an aerosol-assisted route using a novel sol−gel precursor $((PrO^i)_3Si)_2PhSH$ (**1**).[42] Similar to the results of Brinker et al., who have originally introduced the spray method for mesoporous particles made of pure silica, there is an enormous polydispersity regarding particle size.[43] Without further fractionation, it is very difficult to prepare homogeneous nanoparticle films, and further disadvantages of the method are that the overall yield of particles is low. Redispersing the particles in water is hard due to reduced colloidal stability. These problems do not occur for mesoporous silica particles prepared from solution via a modified Stoeber method, as was, for instance, nicely shown by Bein et al.[44] Therefore, it would be highly desirable to adapt the Stoeber method for the preparation of thiol-containing PMO nanoparticles.[45] The modified Stoeber process reported in the literature, using a single surfactant as a structure directing agent,[46] was adapted using **1** as a PMO precursor. Unfortunately, none of the literature procedures could be used for the successful preparation of PMO-MSNs, which is compared to TEOS presumably due to the altered hydrolysis rates of the isopropoxysilyl groups in **1** and differences in polarity because of the slightly hydrophobic character of the thiophenyl group. Cetlytrimethylammonium bromide (CTAB) as a surfactant leads to a polydisperse sample of spherical particles, but neither via transmission electron microscopy (TEM) nor N_2-physisorption measurements could any porosity be detected; see Figure S-1a. Some porous structures with ill-defined pore-systems and ill-defined particles could be obtained, when using the nonionic Brij-56 surfactant (see Figure S-1b). Consequently, an adjustment of the Stoeber process is necessary, and finally a two-step, two surfactant strategy was successful. In the first step, the precursor **1** is hydrolyzed in an acidic isopropanol/water solution (pH = 1.5) by heating for several hours. The warm solution then was poured into a buffered surfactant containing solution and aged for 5 days. Interestingly, already a very low amount of CTAB has a significant effect. Formation of some spherical particles (see Figure S-2a) with internal cavities occurs. The latter results indicate that CTAB is mainly responsible for the stabilization of the growing, colloidal particles. The CTAB to Brij ratio was optimized to 2.6. The entire organosilica material is present in the form of particles having the desired meso-structure seen in TEM (see also Figure S-2b). The latter experiments indicate how complex it is to establish an adequate synthesis for PMO nanoparticles. The structure directing agent was removed via liquid−liquid extraction, and the resulting, porous particles (UKON-2jNP) were characterized in further detail. The data are summarized in Figures 1 and S-3. Nanoparticles with diameters between 70 and 120 nm are present with a fairly narrow size-distribution function as was also seen from scanning electron microscopy (SEM) images (Figure S-3a) and dynamic light scattering (DLS) data (Figure 1c). The particles form stable dispersions in water (Figure S-3b).

The high porosity of the nanoparticles is nicely demonstrated in TEM (Figure 1a). However, as compared to other materials prepared using CTAB or Brij-56, which have pore-sizes in the range ∼3 nm,[47,48] we find that the pores of our material are smaller ($D_{pore} \approx 2$ nm). This is supported by N_2-physisorption measurements given in Figure S-3c. The isotherm is in agreement with the so-called supermicroporous regime with pore-sizes in the range 1.5−2 nm. In addition, in small-angle X-ray scattering (SAXS) (Figure 1b), one sees a signal at $q = 2.08$ nm^{-1}, which corresponds to a value for the pore-to-pore distance of only 3.1 nm. We assume that the hydrolyzed form of the precursor **1** might have slight amphiphilic properties, and that this could influence the hydrophilic−hydrophobic balance of the liquid crystalline structure necessary for the formation of the pores. However, a large advantage of the small pores combined with the high porosity is that the material is characterized by an extraordinarily high internal surface area (A_{BET} = 1400 m^2/g). The chemical composition of the nanoporous UKON-2j particles was determined by a combination of methods (see Figure S-3), also solid-state NMR. The Si to S ratio, detected via EDX measurements (Figure S-3d), fits perfectly with the value expected for UKON-2j (2:1), and also the FT-IR spectrum is in full agreement with UKON-2j.[42] The amount of chemically accessible thiol groups in UKON-2jNP is determined by using the so-called Ellman assay protocol. In a typical reaction, the Ellman reagent (5,5′-dithiobis(2-nitrobenzoic acid)) reacts with free thiol functionalities by cleaving its disulfide bond to give 2-nitro-5-thiobenzoate (TNB), which has a yellow color. Quantification

DOI: 10.1021/jacs.5b12073
J. Am. Chem. Soc. 2016, 138, 3076−3084

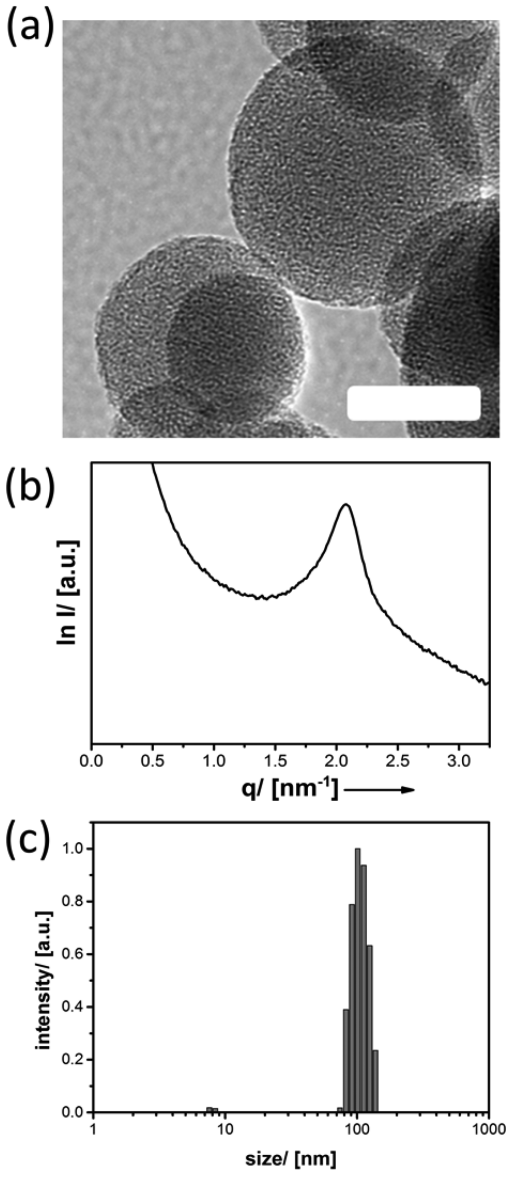

Figure 1. (a) TEM image of UKON-2j nanoparticles prepared via a modified Stoeber process; scale bar = 50 nm; (b) small-angle X-ray scattering (SAXS) data of UKON-2j nanoparticles; and (c) dynamic light scattering analysis of colloidal stable UKON-2j nanoparticle solution.

of TNB is performed by UV/vis measurements and the Beer–Lambert law (ε(TNB) = 1.415 × 10^4 M^{-1} cm^{-1}). As a result (see also Figure S-4), we can conclude that 78% of all thiol groups in the material are accessible and available for further chemical modification. One can now proceed to attach the desired functional entities as shown in Scheme 1. Nitric oxide should be immobilized via *S*-nitrosothiol groups (leading to the material UKON-2jNO), and the ROS producing photosensitizer Rose Bengal will be attached via thiol–ene click chemistry (UKON-2jRB).

***S*-Nitrosothiol Modification on UKON-2j Nanoparticles.** The conversion of UKON-2j to UKON-2jNO (see Scheme 1) can be achieved very easily via the reaction of the thiol groups with $NaNO_2$ in acidic solution. Figure 2a represents the UV/vis data for the Ellmans experiment before and after loading with NO species. Within 4 h, less than 5% of free thiol functionalities in UKON-2jNP remains. As compared to the starting material UKON-2j, a new band in FT-IR appears at 1632 cm^{-1} (see Figure S-5). This band can be assigned to the N═ O stretching vibration of the SNO entities. Elemental analysis of UKON-2jNO shows that the ratio of S:N is 1:0.7, which is very close to the maximum of chemically accessible thiol functions.

Because the activation energy needed for the homolytic dissociation of the S–NO bond is moderate (~150 kJ/mol), depending on the organic rest attached to the sulfur atom, different routes have been established in literature for its cleavage: thermal, catalyzed by copper, or triggered by light.[49] By far, the fastest and most effective way to set the NO radical free is the use of light.[50] As compared to the unmodified thiol, the HOMO–LUMO absorption band is shifted to the VIS spectral region.[49] Absorption of light leads to the population of antibonding σ^* orbitals, bond order decreasing leading to dissociation, and release of NO radicals.[51] Therefore, the next important question is if NO can also be released from UKON-2jNO by light. For testing, we used a solar-simulator (AM-1.5) to mimic natural light. Because of the paramagnetic character of NO, its formation can be traced using electron spin resonance (EPR) spectroscopy. The EPR experiment has been performed under physiological conditions to gather information about the real-time NO release relevant for the biological tests described further below. Because NO is very reactive with a short lifespan, phenylbutylnitrone (PBN) has been used as a spin trap molecule. After the reaction with NO, a group of signals can be observed as a function of time.[52] Figure 2b illustrates the time-dependent evolution of this signal. With increasing light exposure time, one observes that the intensity of the EPR signal increases as well.

The NO release can be quantified more precisely using the Griess assay protocol.[53] The Griess reagent reacts with NO_2^-, which is the major product of nitric oxide deactivation in aqueous solutions. The resulting coloration is quantified using UV/vis spectroscopy, and one can conclude about the initial concentration of NO (see also Figure S-6). Using UKON-2jNO nanoparticles, a slight modification has to be made, which is described in detail in the experimental section. Our investigations (Figure 2c) confirm the results obtained from EPR measurements. The UKON-2jNO material is activated effectively by light, accompanied by a release of NO. NO release is most pronounced during the first hours of irradiation. This is also the most relevant period regarding microbial attachment and initial growth on surfaces. The high concentration of biocidal NO at the beginning guarantees an effective initial attack on microorganism. As compared to the light-induced NO release, the temperature-controlled (T = 35 °C; physiological conditions) pathway is much slower (see Figure 2c). However, the latter experiments underline that the NO release can be tuned with high precision using a combination of light intensity and temperature.

The regeneration of UKON-2jNO material is another important issue. Disulfide bridges (→UKON-2jSS) resulting from the liberation of NO from the nitrosothiol groups in UKON-2jNO (see Figure 3a)[54] can be converted back to –SH (→UKON-2j2) using Clelands reagent.[55] We monitored the cycle of NO release, S–S cleavage, and NO loading by detection of free SH groups employing the previously discussed Ellman assay. Figure 3b shows the corresponding UV/vis spectra in the presence of the different materials. The graphs for UKON-2j, which is a colorless powder (Figure 3b), and UKON-2jNO (green colored solid) are shown again for better

DOI: 10.1021/jacs.5b12073
J. Am. Chem. Soc. 2016, 138, 3076–3084

Scheme 1. Schematic Representation for the Preparation of NO and ROS Releasing Materials[a]

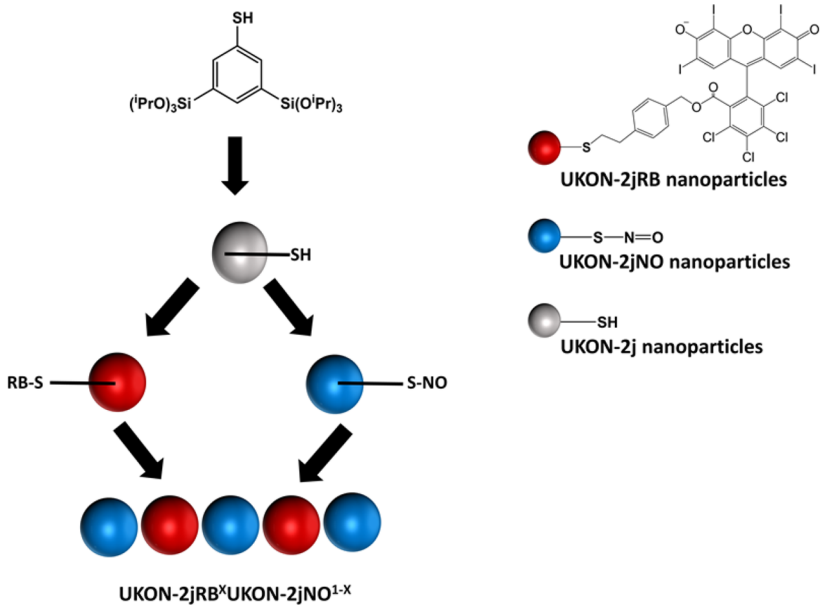

[a]The thiol-containing mesoporous nanoparticles (UKON-2j) are prepared using the corresponding SH precursor in a modified Stoeber process. Post-functionalization of UKON-2j nanoparticles occurs via thiol−ene click reaction for Rose Bengal containing nanoparticles (UKON-2jRB). NO storage is achieved via *S*-nitrosothiol entities (UKON-2jNO). At the bottom the combination of both types of nanoparticle is shown, resulting in the material UKON-2jRB^{x}NO^{1-x}, which can release NO and ROS simultaneously.

comparison. As a consequence of NO binding, the color of UKON-2j has changed from white to brown resulting in UKON-2jNO. After the light-triggered NO release, the color of the resulting material UKON-2jSS is light yellow (UV/vis data shown in S-7), whereas the Ellmann assay documents that there is the same, limited number of residual SH groups present as compared to UKON-2jNO (Figure 3b). After reaction with Clelands reagent, the color of UKON-2j2 as well as the capacity of free thiols then are almost identical to those of UKON-2j, which illustrates the high reversibility.

Rose Bengal Modification of UKON-2j Nanoparticles via Thiol−Ene Click Chemistry. The thiol−ene click reaction offers a fast and effective tool to connect sp^2 hybridized carbon compounds to SH residues by simply using light irradiation or heat.[56] For surface-attachment of Rose Bengal, it was modified with a 4-vinyl-phenyl (VB-RB)[57] group (data given in Figure S-8) and then reacted with UKON-2jNP. After extensive washing for assuring that only covalently linked RB molecules are detected, UV/vis measurements were performed (see Figure 4a). Optical properties of PMO materials can be analyzed very well by a method developed by us and described in a different paper.[35] The UV/vis spectrum of VB-RB is shown as a reference comprising characteristic signals at λ_{max} = 545 nm and a shoulder at 513 nm. Because UKON-2jRB has the same spectral signature, it can be concluded that the Rose Bengal dye is still intact after immobilization and covalent linkage to the thiol groups. According to thermogravimetric analysis data (TGA) seen in Figure 4b, 10% RB could be bound on UKON-2j nanoparticles. This value is very high as compared to other examples for surface-bound RB (~0.03 g RB per g material = 3%).[58] The high modification degree is additionally confirmed by energy dispersive X-ray spectroscopic data (see Figure S-9a). However, it needs to be noted that the observed RB content is still lower, as compared to the quantitative conversion of all thiol functions present in UKON-2j. Because the size of RB can be estimated to be 1.3 nm,[59] which is only slightly smaller than the pore-size (~2 nm), a possibility is that RB bound near the exterior surface of the mesoporous particle aggravates diffusion of additional dye deeper into the particle. Although the wormhole pore-system with highly interconnected pores (Figure 2) is favorable, the described pore-blocking effect cannot be excluded, and there is a remarkable effect on the porosity of the material when RB is immobilized. The corresponding N_2-physisorption isotherms are shown in Figure 4c. The adsorbed volume is shifted to lower values, and also the specific surface area (800 m^2/g) is reduced. The pore-system has not been altered by the modification with RB proven by TEM and SAXS measurements, in which UKON-2jRB (Figure S-9b,c) is identical to UKON-2j (Figure 1a,b).

The disadvantage of free RB is its reduced photostability (see Figure 4d), concluded from time-dependent UV/vis measurements after defined periods of UV light irradiation (see Figure S-10). The covalent binding of RB on UKON-2jNP nanoparticles extends its lifetime significantly and suppresses the self-quenching effect of the dye, resulting from dye*−dye intermolecular reactions, which occur when the distance between two RB molecules is short enough.[60] The capability of UKON-2jRB for ROS production can be monitored quantitatively using the uric acid degradation (UAD) assay.[61] Uric acid is one of the most important, water-soluble antioxidants, which scavenges oxidants like singlet oxygen, nitric oxides, and peroxynitrites.[62] Its absorption maximum is located at 293 nm and can be monitored by UV/vis spectroscopy. Figure S-11 presents the set of UV/vis data after sunlight exposure for different time periods. The presence of UKON-2jRB nanoparticles in the UA solution leads to complete disappearance of the uric acid signal after 10 min of irradiation with visible light. Rossi et al. introduced the concept of $^1O_2$ delivery efficiency η expressed by eq 1:[63−65]

DOI: 10.1021/jacs.5b12073
J. Am. Chem. Soc. 2016, 138, 3076−3084

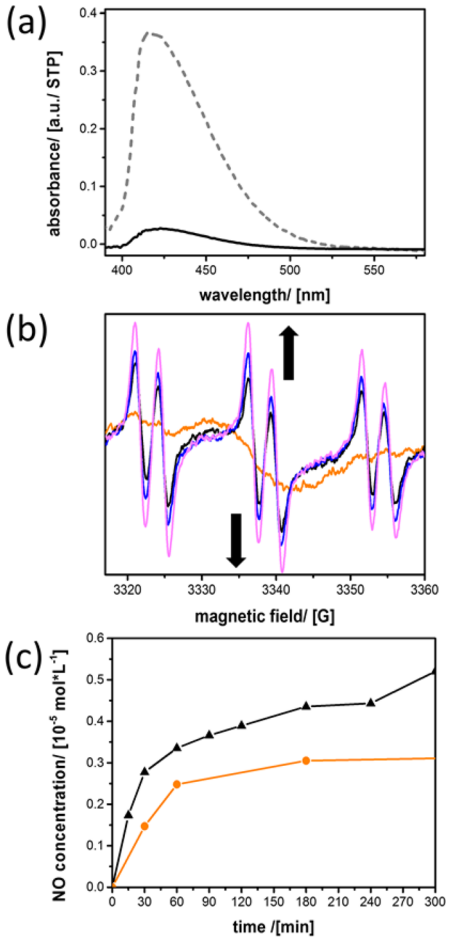

Figure 2. (a) UV/vis spectra of Ellmans reagent before (gray bars) and after (black, solid curve) NO binding on UKON-2jNP. (b) EPR spectra of solutions containing PBN- radicals resulting from the light-induced release of NO from UKON-2jNO irradiated for different time (orange curve, t = 15 min; black curve, t = 45 min; blue curve, t = 75 min; rose curve, t = 120 min). (c) Comparison of NO release induced by sunlight exposure (▲) and temperature (35 °C; orange ●); data obtained from UV/vis measurements via Griess assay.

$$\eta(\text{RB-mat}) = \Phi^{1}O_2 \frac{t(\text{RB})}{t(\text{RB-mat})} \quad (1)$$

where t(RB) is the time for the decrease in absorption of uric acid in the presence of free RB in a aqueous solution (data given in Figure S-10a,b); t(RB-mat) is the time for the decrease in absorption of UA in the presence of immobilized RB on a material in a aqueous solution (data given in Figure S-11); and Φ is the singlet oxygen quantum yield of RB in an aqueous solution (Φ = 0.75). This equation takes into account an irradiation wavelength of 540 nm (λ_{max}(RB)). For UKON-2jRB nanoparticles, the $^1O_2$ delivery efficiency η was calculated considering sunlight with the emission spectra of a solar-simulator (AM-1.5). The resulting $^1O_2$ delivery efficiency value (η = 0.68) is in the range of the singlet oxygen quantum yield of RB, which is remarkable considering the fact that in our system sunlight is used.

Binary Nanoparticle System and Synergistic Effects. Initially a 50:50 mixture UKON-2jNO and UKON-2jRB was explored, and the composite sample is denoted as UKON-2jRB$^{0.5}$NO$^{0.5}$. Figure 5a summarizes the ROS reaction rate (determined via the aforementioned procedures) for the latter material and compares it to the results of the isolated constituents UKON-2jRB and UKON-2jNO. A cooperative effect between UKON-2jRB and UKON-2jNO is clearly observed, which extends beyond a simple superposition of the two systems. Although there is less of the ROS producing UKON-2jRB in the composite, sunlight exposure of UKON-2jRB$^{0.5}$NO$^{0.5}$ leads to a significantly faster uric acid degradation as compared to UKON-2jRB alone. As it is irrational that more ROS species are produced by UKON-2jRB$^{0.5}$NO$^{0.5}$, a more effective species as compared to the isolated systems must be generated. Superoxide $O_2^{\bullet-}$, resulting from UKON-2jRB, can react with NO released from UKON-2jNO resulting in the peroxynitrite ion ($ONOO^-$).[66] For more specific peroxynitrite detection, we used dihydrorhodamine 123 (DHR) as a nonfluorescent molecule, which by oxidation forms rhodamine 123 (RH) (λ_{abs} = 505 nm).[67] Figure 5c shows the results. No difference can be seen between the spectra of DHR irradiated and dissolved in aqueous solution as a reference and DHR in the presence of UKON-2jNO. Without the ROS species produced from UKON-2jRB, no peroxynitrite species are detected. In contrast to this, for UKON-2jRB$^{0.5}$NO$^{0.5}$, the presence of peroxynitrite is clearly proven by the pronounced signal for RH.

One tremendous advantage of the peroxynitrite anion is its good stability in aqueous solutions (half-life time 10−20 ms). Because of quantitative diffusion through cell walls, it is

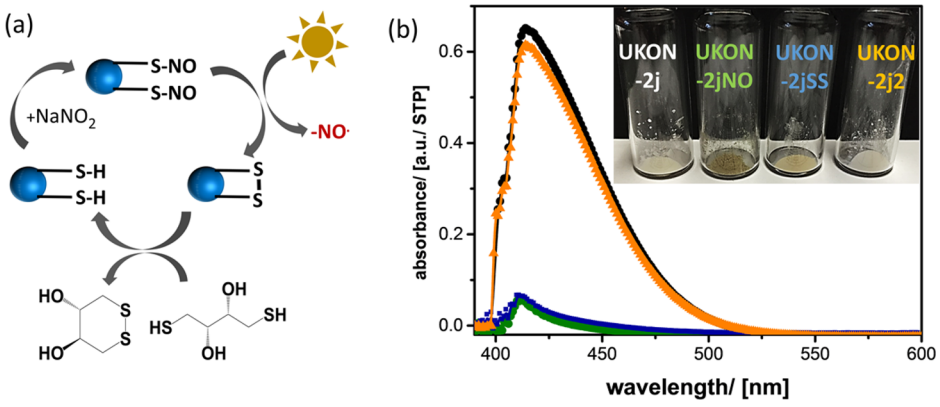

Figure 3. (a) Illustration of recycling UKON-2j for repeated NO loading and release. (b) UV/vis data of Ellmans assay and photographic images of UKON-2j (●), UKON-2jNO (green ■), UKON-2jSS (blue ■), and UKON-2j2 (orange ▲).

DOI: 10.1021/jacs.5b12073
J. Am. Chem. Soc. 2016, 138, 3076−3084

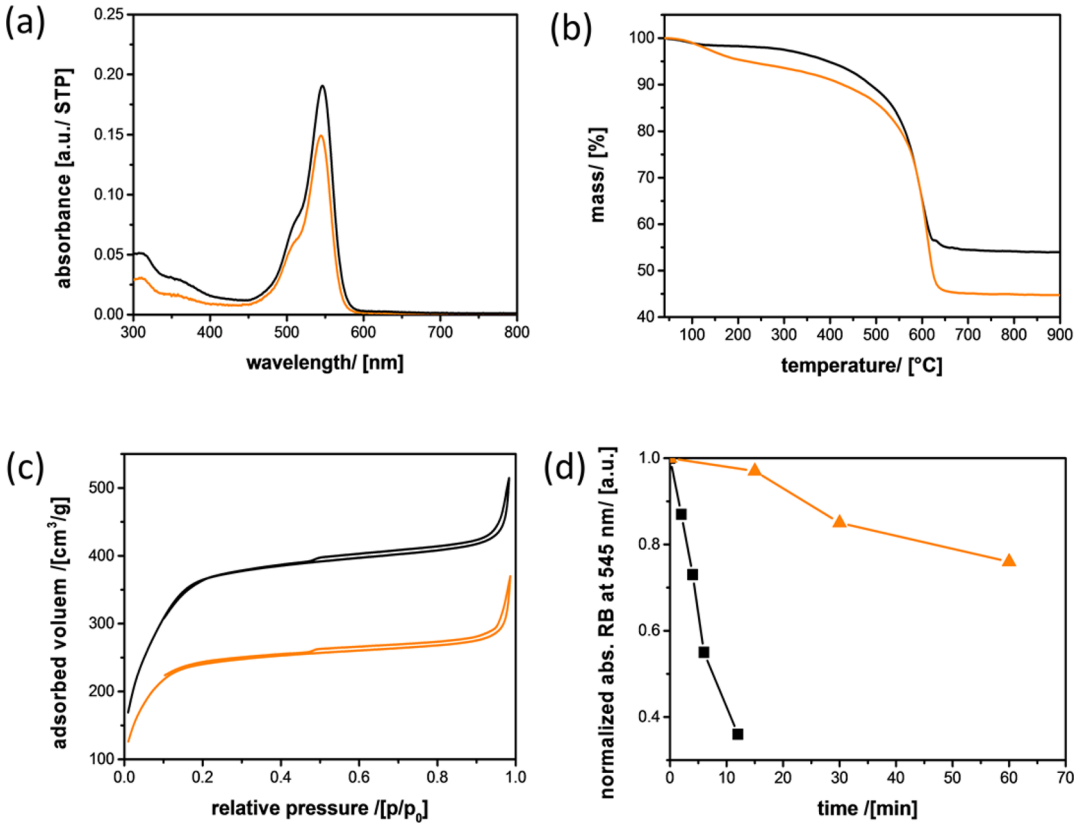

Figure 4. (a) UV/vis data of pure VB-RB (black curve) as a reference and UKON-2jRB (orange curve). (b) TGA data of UKON-2j (black curve) and UKON-2jRB (orange curve). (c) N_2-physisorption data of UKON-2j nanoparticles (black curve) having the BET surface area of 1400 m^2/g and Rose Bengal hosting UKON-2jRB nanoparticles (orange curve) with BET surface area of 800 m^2/g. (d) Photostability of molecular RB as a reference (■) and immobilized in UKON-2jRB (orange ▲) as a function of time.

expected that it will destroy cellular constituents effectively, leading to dysfunction of important cellular processes and inducing cell death.[68] Before we conduct the biological tests, it is important to determine which ratio of UKON-2jRB to UKON-2NO nanoparticles exhibits the best performance (Figure 5b). Within the investigated series, UKON-2jRB$^{0.25}$NO$^{0.75}$ is most effective, and this shows that the performance of released NO can be maximized by only a small amount of UKON-2jRB present.

Evaluation of Biocidal Activity. All compounds (NO, ROS, peroxynitrite) released from the different materials via light irradiation are expected to exhibit biocidal activity. The mechanism of NO, ROS, and peroxynitrite species in tissue damaging processes ranges from protein oxidation and nitration, lipid peroxidation, to inactivation of enzymes, to mention only a few of them.[69] Because their mode of operation is, unlike antibiotics, very broad and no target molecules are specifically addressed, the risk of potential resistance development against one of these highly reactive species is very low. To qualitatively evaluate the antibacterial activity of the nanoparticles presented in this study, the following experiment was performed: The biocidal properties of nanoparticle dispersions were tested in nutrient medium (LB medium), using suspended cells of the opportunistic pathogenic bacterium *Pseudomonas aeruginosa* as a model. One milligram of pure UKON-2jRB or UKON-2jNO particles, or a combination of both particles (UKON-2jRB$^{0.25}$NO$^{0.75}$), was mixed with bacterial cells and nutrient medium (1 mL). The suspensions were exposed to simulated sunlight, and at time intervals (0, 15, 30, 60, 120, and 180 min), samples were taken, serially diluted, and drop-plated onto nutrient agar plates, to determine colony-forming units (CFU) (see Figure 6). In the control experiment, the viability (CFU) of the cell population remained about constant during the experiment, indicating that the light exposure alone had no effect on the bacteria. For the treatments with nanoparticles, the presence of UKON-2jNO was the least effective, followed by UKON-2jRB. However, the combination of nanoparticles, UKON-2jRB$^{0.25}$NO$^{0.75}$, leads to a significant reduction of viable bacteria over time. Therefore, it can be concluded that there is not only a synergistic effect through the combination of particles with respect to uric acid degradation, as discussed above, but that the simultaneous release of NO and ROS species in one system also leads to advanced biocidal activity. However, it needs to be marked that the latter experiments represent only a first proof-of-concept, which needs to be complemented by additional tests (see below). A viability of 10% is yet too high for granting sufficient antibacterial protection. For a dispersion of the mesoporous particles in water, there is neither the desired, close proximity of the both types of nanoparticles to each other, nor a satisfactory proximity of the bacteria to the nanoparticles. As a consequence, the local concentration of peroxynitrite is low.

Consequently, one needs to check if the biocidal activity changes for bacteria brought to a densely packed film of nanoparticles (see Figures 7a and S-13). Prior to use, the glass slides were cleaned and hydroxylated using peroxo sulfuric acid. The stability of the nanoparticle film was tested after immersing the covered glass slides in water and storage for several weeks.

DOI: 10.1021/jacs.5b12073
J. Am. Chem. Soc. 2016, 138, 3076−3084

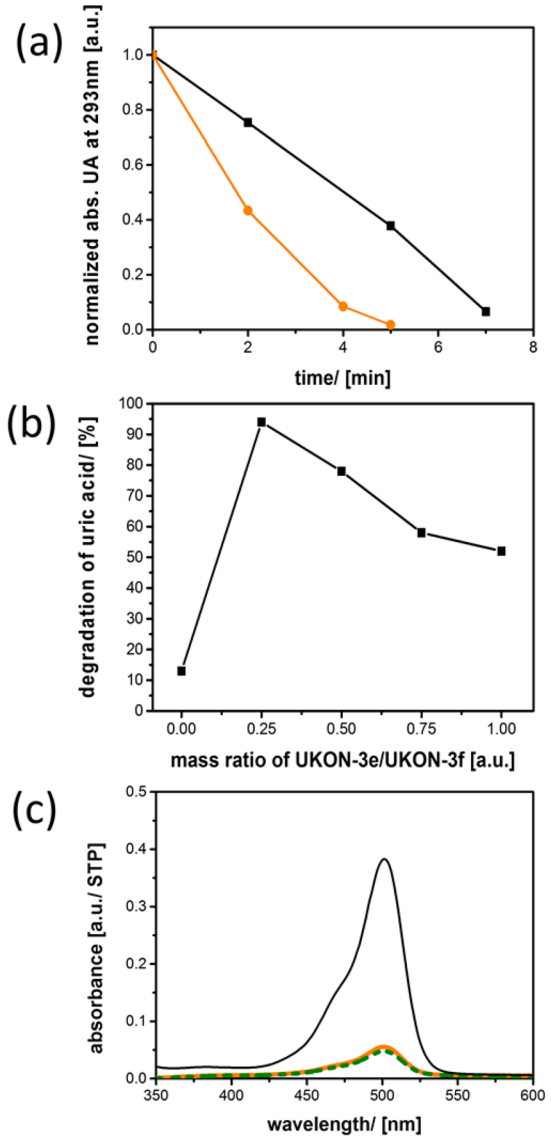

Figure 5. (a) ROS rate determined via the UAD essay for UKON-2jRB (■) and UKON-2jRB$^{0.5}$NO$^{0.5}$ (orange ●). (b) Uric acid degradation in % for the binary PMO nanoparticle system UKON-2jRB^{x}NO^{1-x} after 4 min of sunlight exposure. (c) UV/vis spectra of Rhodamine 123 (RH) formed by sunlight exposure for 1 h and UKON-2jRB$^{0.5}$NO$^{0.5}$ (black curve), UKON-2jNO (orange curve), and pure dihydrorhodamine 123 (DHR) solution (green dashed).

No detachment of the nanoparticles was observed, also after washing the nanoparticle films with water. For the evaluation of the disinfection efficiency of the nanoparticles, bacterial cell suspension (*P. aeruginosa*; 10^9 CFU/ml) was soaked into the nanoparticle films, followed by incubation for 1 h under irradiation by simulated sunlight. The films then were imprinted on nutrient agar plates (LB medium), followed by incubation of the plates for 24 h at 30 °C in the dark (see Figure 7b).

Figure 7c,d shows the resulting agar plates after incubation, indicating bacterial growth as macroscopically visible lawns. The antibacterial properties can be switched on and off by light, which is an important requisite for an aPDT material. In the absence of light, there is strong bacterial growth for all three systems, UKON-2jNO^{100}, UKON-2jRB^{100}, and UKON-2jRB$^{0.25}$NO$^{0.75}$ (Figure 7c). However, with only 1 h of

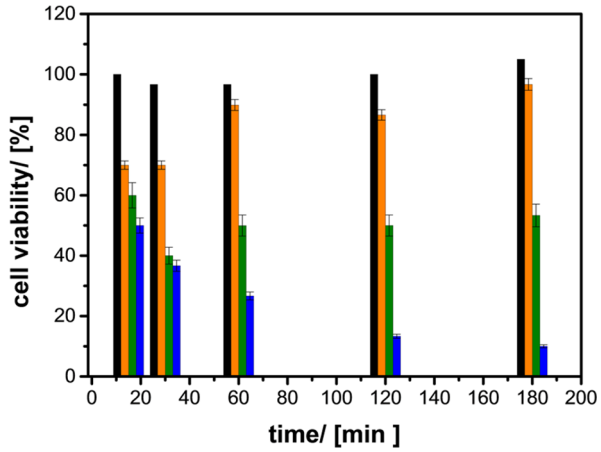

Figure 6. Time dependence of biocidal action against suspended cells of *P. aeruginosa* for treatments with simulated sunlight alone as a reference (black columns), and for treatments with simulated sunlight in the presence of suspended nanoparticles of UKON-2jNO (orange columns), UKON-2jRB (green columns), and UKON-2jRB$^{0.25}$NO$^{0.75}$ (blue columns) materials. Error bars represent standard deviation (n = 3). A logarithmic plot is given in Figure S-12.

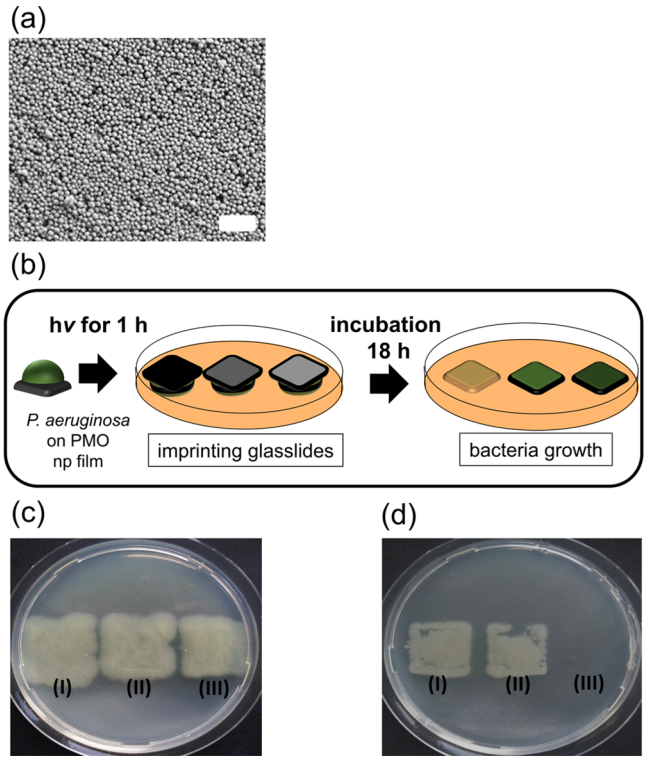

Figure 7. (a) Representative SEM image of PMO nanoparticle films on glass slides; scale bar, 1 μm. (b) Schematic illustration of a photo initiated disinfection assay when using UKON nanoparticle films and *P. aeruginosa*. Nutrient agar plates were locally imprinted with glass slides coated with UKON-2jRB (I), UKON-2jNO (II), or UKON-2jRB$^{0.25}$NO$^{0.75}$ (III) nanoparticle films, which had been "contaminated" with bacteria (*P. aeruginosa*). (c) No sunlight illumination of the UKON nanoparticle films after contamination. (d) After illumination with sunlight for 1 h.

irradiation with sunlight (Figure 7d), the materials UKON-2jNO^{100} and UKON-2jRB^{100} lead to a significant reduction of bacterial growth due to NO and ROS release, respectively, but they did not prevent growth completely. Only with UKON-

DOI: 10.1021/jacs.5b12073
J. Am. Chem. Soc. 2016, 138, 3076−3084

$2jRB^{0.25}NO^{0.75}$ was a complete inhibition of bacterial growth observed.

CONCLUSION

In the current contribution, four challenges were mastered leading to a novel, silver-free material with enhanced biocidal activity. First, we were able to adopt the Stoeber process for the preparation of highly functional organosilica nanoparticles of the thiol-PMO type with narrow size distribution. It could be shown that the thiol groups present inside these particles are highly accessible and can be converted to other functional groups almost quantitatively. One possibility was to covalently anchor NO, whose release could be triggered by light. Alternatively, Rose Bengal was attached to the pore surfaces of the PMO nanoparticles using thiol−ene click chemistry. The photochemical production of reactive oxygen species was investigated. In the last step, we could verify that the binary system, comprised of particles of both types, exhibits a cooperative effect concerning biocidal activity tested on *P. aeruginosa* as a bacterial model system. This unique synergy between the two particles is due to the formation of peroxynitrite, which possesses an improved capability to infiltrate bacterial cells. In the future, it will be important to standardize the data obtained here with antibiofilm experiments known from the literature. Unfortunately, it is not possible yet to adapt standard procedures like ASTM E2180 directly, due to the porous and particle-like character of our samples. As cell adhesion on porous surfaces represents a central issue, separate efforts need to be taken to develop suitable standardization techniques for porous films. Herein, we adopt the semi-quantitative imprinting method reported by Trobos et al.[70] They extensively discuss the bacteria−material surface interaction regarding the methodological development to evaluate antibacterial effects and came to the conclusion that for the contact killing mechanism, like the presented material, the imprinting method represents the best assay to evaluate antibacterial activity taking cell adhesion into account.

Nevertheless, in comparison to similar light-mediated antibacterial surfaces like TiO_2 films[71] or surface bound photosensitizers,[72] the nanoparticle system discussed in this Article works with VIS-light and at low intensities, and thus it can be applied using ambient light. In medical settings, we envision potential utilization for items, which are exposed to light, and when rapid and immediate antibacterial protection is required, like in bandages, cannulas, or other equipment used for infusions. Because unreacted thiol-groups on the nanoparticles surface can be used for direct surface attachment on different surfaces (e.g., stainless steel),[42] or the particles can be modified with groups binding specifically to certain targets (e.g., cotton, proteins), one can expect that the systems presented here can be applied for a variety of substrates.

ASSOCIATED CONTENT

Supporting Information

The Supporting Information is available free of charge on the ACS Publications website at DOI: 10.1021/jacs.5b12073.

Detailed description of all experimental details, and Figures S1−S13 (PDF)

AUTHOR INFORMATION

Corresponding Author

*sebastian.polarz@uni-konstanz.de

Notes

The authors declare no competing financial interest.

ACKNOWLEDGMENTS

We thank the Alfred-Kärcher Förderstiftung for funding the project.

REFERENCES

(1) Vera, D. M. A.; Haynes, M. H.; Ball, A. R.; Dai, D. T.; Astrakas, C.; Kelso, M. J.; Hamblin, M. R.; Tegos, G. P. *Photochem. Photobiol.* **2012**, *88*, 499.
(2) Lewis, K. *Nat. Rev. Drug Discovery* **2013**, *12*, 371.
(3) Ling, L. L.; Schneider, T.; Peoples, A. J.; Spoering, A. L.; Engels, I.; Conlon, B. P.; Mueller, A.; Schaberle, T. F.; Hughes, D. E.; Epstein, S.; Jones, M.; Lazarides, L.; Steadman, V. A.; Cohen, D. R.; Felix, C. R.; Fetterman, K. A.; Millett, W. P.; Nitti, A. G.; Zullo, A. M.; Chen, C.; Lewis, K. *Nature* **2015**, *517*, 455.
(4) Zheng, Y.; Hu, T.; Chen, C.; Yang, F.; Yang, X. *Chem. Commun.* **2015**, *51*, 5645.
(5) Hasan, J.; Crawford, R. J.; Ivanova, E. P. *Trends Biotechnol.* **2013**, *31*, 295.
(6) Martinez-Gutierrez, F.; Boegli, L.; Agostinho, A.; Sanchez, E. M.; Bach, H.; Ruiz, F.; James, G. *Biofouling* **2013**, *29*, 651.
(7) Panyala, N. R.; Pena-Mendez, E. M.; Havel, J. *J. Appl. Biomed.* **2008**, *6*, 117.
(8) Ragas, X.; He, X.; Agut, M.; Roxo-Rosa, M.; Gonsalves, A. R.; Serra, A. C.; Nonell, S. *Molecules* **2013**, *18*, 2712.
(9) Rajesh, S.; Koshi, E.; Philip, K.; Mohan, A. *J. Indian Soc. Periodontol.* **2011**, *15*, 323.
(10) Cabiscol, E. *Int. Microbiol.* **2010**, *3*, 3.
(11) Gianotti, E.; Martins Estevão, B.; Cucinotta, F.; Hioka, N.; Rizzi, M.; Renò, F.; Marchese, L. *Chem. - Eur. J.* **2014**, *20*, 10921.
(12) Neckers, D. C. *J. Photochem. Photobiol., A* **1989**, *47*, 1.
(13) Valkov, A.; Nakonechny, F.; Nisnevitch, M. *Int. J. Mol. Sci.* **2014**, *15*, 14984.
(14) Wang, B.; Wang, J.-H.; Liu, Q.; Huang, H.; Chen, M.; Li, K.; Li, C.; Yu, X.-F.; Chu, P. K. *Biomaterials* **2014**, *35*, 1954.
(15) Uppal, A.; Jain, B.; Gupta, P. K.; Das, K. *Photochem. Photobiol.* **2011**, *87*, 1146.
(16) Perni, S.; Prokopovich, P.; Pratten, J.; Parkin, I. P.; Wilson, M. *Photochem. Photobiol. Sci.* **2011**, *10*, 712.
(17) Koh, A.; Carpenter, A. W.; Slomberg, D. L.; Schoenfisch, M. H. *ACS Appl. Mater. Interfaces* **2013**, *5*, 7956.
(18) Shin, J. H.; Metzger, S. K.; Schoenfisch, M. H. *J. Am. Chem. Soc.* **2007**, *129*, 4612.
(19) Riccio, D. A.; Nugent, J. L.; Schoenfisch, M. H. *Chem. Mater.* **2011**, *23*, 1727.
(20) Li, Z.; Barnes, J. C.; Bosoy, A.; Stoddart, J. F.; Zink, J. I. *Chem. Soc. Rev.* **2012**, *41*, 2590.
(21) Egger, S. M.; Hurley, K. R.; Datt, A.; Swindlehurst, G.; Haynes, C. L. *Chem. Mater.* **2015**, *27*, 3193.
(22) Hoffmann, F.; Cornelius, M.; Morell, J.; Fröba, M. *Angew. Chem., Int. Ed.* **2006**, *45*, 3216.
(23) Vallet-Regí, M.; Balas, F.; Arcos, D. *Angew. Chem., Int. Ed.* **2007**, *46*, 7548.
(24) Sanchez, C.; Julian, B.; Belleville, P.; Popall, M. *J. Mater. Chem.* **2005**, *15*, 3559.
(25) Inagaki, S.; Guan, S.; Fukushima, Y.; Ohsuna, T.; Terasaki, O. *J. Am. Chem. Soc.* **1999**, *121*, 9611.
(26) Melde, B. J.; Holland, B. T.; Blanford, C. F.; Stein, A. *Chem. Mater.* **1999**, *11*, 3302.
(27) Asefa, T.; MacLachlan, M. J.; Coombs, N.; Ozin, G. A. *Nature* **1999**, *402*, 867.
(28) Niu, D.; Liu, Z.; Li, Y.; Luo, X.; Zhang, J.; Gong, J.; Shi, J. *Adv. Mater.* **2014**.
(29) Croissant, J.; Cattoen, X.; Wong Chi Man, M.; Dieudonne, P.; Charnay, C.; Raehm, L.; Durand, J. O. *Adv. Mater.* **2015**, *27*, 145.

DOI: 10.1021/jacs.5b12073
J. Am. Chem. Soc. 2016, 138, 3076−3084

(30) Ide, M.; De Canck, E.; Van Driessche, I.; Lynen, F.; Van der Voort, P. *RSC Adv.* **2015**, *5*, 5546.
(31) Kuschel, A.; Polarz, S. *J. Am. Chem. Soc.* **2010**, *132*, 6558.
(32) Kuschel, A.; Polarz, S. *Adv. Funct. Mater.* **2008**, *18*, 1272.
(33) Kuschel, A.; Drescher, M.; Kuschel, T.; Polarz, S. *Chem. Mater.* **2010**, *22*, 1472.
(34) Schachtschneider, A.; Wessig, M.; Spitzbarth, M.; Donner, A.; Fischer, C.; Drescher, M.; Polarz, S. *Angew. Chem.* **2015**, *127*, 10611.
(35) Luka, M.; Polarz, S. *Microporous Mesoporous Mater.* **2013**, *171*, 35.
(36) Gehring, J.; Schleheck, D.; Trepka, B.; Polarz, S. *ACS Appl. Mater. Interfaces* **2015**, *7*, 1021.
(37) Gehring, J.; Schleheck, D.; Luka, M.; Polarz, S. *Adv. Funct. Mater.* **2014**, *24*, 1140.
(38) Esquivel, D.; van den Berg, O.; Romero-Salguero, F. J.; Du Prez, F.; Van Der Voort, P. *Chem. Commun.* **2013**, *49*, 2344.
(39) Tang, F.; Li, L.; Chen, D. *Adv. Mater.* **2012**, *24*, 1504.
(40) Zhang, Q.; Wang, X.; Li, P.-Z.; Nguyen, K. T.; Wang, X.-J.; Luo, Z.; Zhang, H.; Tan, N. S.; Zhao, Y. *Adv. Funct. Mater.* **2014**, *24*, 2413.
(41) Lu, Y.; Shah, A.; Hunter, R. A.; Soto, R. J.; Schoenfisch, M. H. *Acta Biomater.* **2015**, *12*, 62.
(42) Gehring, J.; Schleheck, D.; Trepka, B.; Polarz, S. *ACS Appl. Mater. Interfaces* **2014**.
(43) Lu, Y.; Fan, H.; Stump, A.; Ward, T. L.; Rieker, T.; Brinker, C. J. *Nature* **1999**, *398*, 223.
(44) Möller, K.; Kobler, J.; Bein, T. *Adv. Funct. Mater.* **2007**, *17*, 605.
(45) Zhang, Y.; Hsu, B. Y. W.; Ren, C.; Li, X.; Wang, J. *Chem. Soc. Rev.* **2015**, *44*, 315.
(46) Guan, B.; Cui, Y.; Ren, Z.; Qiao, Z.-a.; Wang, L.; Liu, Y.; Huo, Q. *Nanoscale* **2012**, *4*, 6588.
(47) Wang, A.; Kabe, T. *Chem. Commun.* **1999**, 2067.
(48) Coleman, N. R. B.; Attard, G. S. *Microporous Mesoporous Mater.* **2001**, *44*−*45*, 73.
(49) Singh, R. J.; Hogg, N.; Joseph, J.; Kalyanaraman, B. *J. Biol. Chem.* **1996**, *271*, 18596.
(50) Wang, P. G.; Xian, M.; Tang, X.; Wu, X.; Wen, Z.; Cai, T.; Janczuk, A. J. *Chem. Rev.* **2002**, *102*, 1091.
(51) Ruano, C.; Otero, J. C.; Arenas, J. F.; Soto, J. *Chem. Phys. Lett.* **2012**, *553*, 17.
(52) Villamena, F. A.; Zweier, J. L. *Antioxid. Redox Signaling* **2004**, *6*, 619.
(53) Zhang, H.; Annich, G. M.; Miskulin, J.; Stankiewicz, K.; Osterholzer, K.; Merz, S. I.; Bartlett, R. H.; Meyerhoff, M. E. *J. Am. Chem. Soc.* **2003**, *125*, 5015.
(54) Kim, J.; Saravanakumar, G.; Choi, H. W.; Park, D.; Kim, W. J. *J. Mater. Chem. B* **2014**, *2*, 341.
(55) Croissant, J.; Cattoen, X.; Man, M. W. C.; Gallud, A.; Raehm, L.; Trens, P.; Maynadier, M.; Durand, J. O. *Adv. Mater.* **2014**, *26*, 6174.
(56) Lowe, A. B. *Polym. Chem.* **2010**, *1*, 17.
(57) Zhang, W.; Vinueza, N. R.; Datta, P.; Michielsen, S. *J. Polym. Sci., Part A: Polym. Chem.* **2015**, *53*, 1594.
(58) Martins Estevao, B.; Cucinotta, F.; Hioka, N.; Cossi, M.; Argeri, M.; Paul, G.; Marchese, L.; Gianotti, E. *Phys. Chem. Chem. Phys.* **2015**, *17*, 26804.
(59) Bang, G. S.; Park, J.; Lee, J.; Choi, N.-J.; Baek, H. Y.; Lee, H. *Langmuir* **2007**, *23*, 5195.
(60) Paczkowski, J.; Neckers, D. C. *Macromolecules* **1985**, *18*, 2412.
(61) Fischer, F.; Graschew, G.; Sinn, H. J.; Maier-Borst, W.; J. Lorenz, W.; Schlag, P. M. *Clin. Chim. Acta* **1998**, *274*, 89.
(62) Gersch, C.; Palii, S. P.; Imaram, W.; Kim, K. M.; Karumanchi, S. A.; Angerhofer, A.; Johnson, R. J.; Henderson, G. N. *Nucleosides, Nucleotides Nucleic Acids* **2009**, *28*, 118.
(63) Rossi, L. M.; Silva, P. R.; Vono, L. L. R.; Fernandes, A. U.; Tada, D. B.; Baptista, M. S. *Langmuir* **2008**, *24*, 12534.
(64) Silva, P. R.; Vono, L. L. R.; Esposito, B. P.; Baptista, M. S.; Rossi, L. M. *Phys. Chem. Chem. Phys.* **2011**, *13*, 14946.
(65) Martins Estevao, B.; Cucinotta, F.; Hioka, N.; Cossi, M.; Argeri, M.; Paul, G.; Marchese, L.; Gianotti, E. *Phys. Chem. Chem. Phys.* **2015**, *17*, 26804.
(66) Szabo, C.; Ischiropoulos, H.; Radi, R. *Nat. Rev. Drug Discovery* **2007**, *6*, 662.
(67) Gomes, A.; Fernandes, E.; Lima, J. L. F. C. *J. Biochem. Biophys. Methods* **2005**, *65*, 45.
(68) Pacher, P.; Beckman, J. S.; Liaudet, L. *Physiol. Rev.* **2007**, *87*, 315.
(69) Virág, L.; Szabó, É.; Gergely, P.; Szabó, C. *Toxicol. Lett.* **2003**, *140*−*141*, 113.
(70) Zaborowska, M.; Welch, K.; Brånemark, R.; Khalilpour, P.; Engqvist, H.; Thomsen, P.; Trobos, M. *J. Biomed. Mater. Res., Part B* **2015**, *103*, 179.
(71) Pleskova, S. N.; Golubeva, I. S.; Verevkin, Y. K. *Mater. Sci. Eng., C* **2016**, *59*, 807.
(72) Cahan, R.; Schwartz, R.; Langzam, Y.; Nitzan, Y. *Photochem. Photobiol.* **2011**, *87*, 1379.

DOI: 10.1021/jacs.5b12073
J. Am. Chem. Soc. 2016, 138, 3076−3084